

1 Mechanistic Insights on the Light-Driven Catalysis  
2 of an Immobilized Lipase on Plasmonic  
3 Nanomaterials

4 *Heloise Ribeiro de Barros,\*<sup>a,b</sup> Isabel García,<sup>b,c</sup> Christian Kuttner,<sup>b</sup> Nicoll Zeballos,<sup>b</sup> Pedro H.*  
5 *C. Camargo,<sup>a,d</sup> Susana Inés Cordoba de Torresi,<sup>a</sup> Fernando López-Gallego,\*<sup>b,e</sup> and Luis M. Liz-*  
6 *Marzán<sup>b,c,e</sup>*

7 <sup>a</sup> Department of Fundamental Chemistry, Institute of Chemistry, University of São Paulo, Av.  
8 Prof. Lineu Prestes, 748, Vila Universitária, 05508-000 São Paulo, SP, Brazil.

9 <sup>b</sup> CIC biomaGUNE, Basque Research and Technology Alliance (BRTA), Paseo de Miramón  
10 182, 20014 Donostia – San Sebastián, Spain.

11 <sup>c</sup> Centro de Investigación Biomédica en Red, Bioingeniería, Biomateriales y Nanomedicina  
12 (CIBER-BBN), Paseo de Miramón 182, 20014 Donostia – San Sebastián, Spain.

13 <sup>d</sup> Department of Chemistry, University of Helsinki, A.I. Virtasen aukio 1, Helsinki, Finland

14 <sup>e</sup> Ikerbasque, Basque Foundation for Science, 48013 Bilbao, Spain.

15 KEYWORDS biocatalysis, gold nanostructures, LSPR-enhanced mechanisms, nanotechnology,  
16 plasmonic heating, triggered bioactivity.

## 17 ABSTRACT

18 The use of light as an external stimulus to control enzyme activity is an emerging strategy that  
19 enables accurate, remote and noninvasive biotransformations. In this context, immobilization of  
20 enzymes on plasmonic nanoparticles offers an opportunity to create light-responsive biocatalytic  
21 materials. Nevertheless, a fundamental and mechanistic understanding on the effects of localized  
22 surface plasmon resonance (LSPR) excitation over enzyme regulation remains elusive. We  
23 investigate herein the plasmonic effects on biocatalysis using Au nanospheres (AuNSp) and  
24 nanostars (AuNSt) as model plasmonic nanoparticles, lipase from *Candida antarctica* fraction B  
25 (CALB) as a proof of concept enzyme, and 808 nm as NIR light excitation. Our data show that  
26 LSPR excitation enables an enhancement of 58% in enzyme activity for CALB adsorbed on  
27 AuNSt, compared with the dark conditions. This work shows how photothermal heating over the  
28 LSPR excitation enhances CALB activity through favoring product release in the last step of the  
29 enzyme mechanism. We propose that the results reported herein shed important mechanistic and  
30 kinetic insights in the field of plasmonic biocatalysis and may inspire the rational development of  
31 plasmonic nanomaterial-enzyme hybrids with tailored activities under external light irradiation.

32

## 33 INTRODUCTION

34 Plasmonic nanomaterials, such as gold nanoparticles (Au NPs), display remarkable optical  
35 properties in the visible and near-infrared (NIR) spectral regions.<sup>1-3</sup> Such properties arise as a result  
36 of the excitation of localized surface plasmon resonances (LSPRs). It has been established that  
37 LSPR excitation in plasmonic NPs can accelerate a myriad of chemical transformations.<sup>4-7</sup> This

38 catalytic effect can occur as a result of the generation of LSPR-excited charge carriers (hot  
39 electrons and hot holes) and/or photothermal heating following plasmon decay.<sup>4, 8, 9</sup> Surprisingly,  
40 only a few studies have explored the use of LSPR excitation to tune biocatalytic reactions.<sup>10-15</sup>

41 The conjugation of enzymes to plasmonic NPs is attractive for applications in biomedicine,  
42 such as photothermal therapy<sup>16, 17</sup> and bioimaging,<sup>18</sup> as well as in chemical manufacturing.<sup>13</sup> In  
43 fact, the use of plasmonic effects at the interface between nanoparticles and enzymes is gaining  
44 momentum as a tool to remotely control biocatalytic processes using light as an external  
45 stimulus.<sup>12, 13, 19</sup> This field, plasmonic biocatalysis, paves the way to tuning enzymes' properties in  
46 a non-invasive manner, enabling spatio-temporal control over the biocatalytic processes.<sup>12, 13</sup>  
47 Despite these fascinating opportunities, the mechanisms at the “nano-bio” interface underlying the  
48 influence of plasmonic effects on enzyme functionality are poorly understood.<sup>10, 12, 20</sup>

49 What is already known is that the enzyme/nanomaterial interface plays an important role  
50 in the transport of substrates and products from the bulk to the enzyme active site, and *vice versa*,  
51 thereby altering enzyme activity.<sup>21</sup> For example, recent insightful mechanistic studies revealed that  
52 the conjugation of hydrolases (*i.e.* phosphotriesterase) to quantum dots and Au NPs enhances the  
53 enzymatic kinetic efficiency, as compared to their free counterparts.<sup>22, 23</sup> Furthermore, kinetic  
54 studies under high viscosity conditions demonstrate that the increase in apparent catalytic rate ( $k_{cat}$ )  
55 relies on higher product release kinetic constants associated to the last step of the hydrolases  
56 catalytic mechanism. Nevertheless, how those kinetic parameters may be altered by light at the  
57 interface between enzyme and plasmonic nanomaterials is still an open question that remains  
58 largely underexplored.

59 To bridge this gap, we report herein on a detailed and systematic study of the effects of  
60 LSPR excitation over the activity and enhancement mechanisms in plasmonic biocatalysis.  
61 Specifically, we selected the lipase from *Candida antarctica* fraction B (CALB) as a proof of  
62 concept enzyme, whose catalytic mechanism is well understood, Au nanospheres (AuNSp) and  
63 nanostars (AuNSt) as model plasmonic NPs, and a NIR laser as the light excitation source. Both  
64 on- (AuNSs) and off- (AuNPs) resonance conditions relative to the NIR laser source were  
65 investigated to demonstrate the LSPR-driven enhancement effects. Although CALB has been  
66 previously conjugated to Au NPs,<sup>24-26</sup> control over its catalytic activity through plasmonic effects  
67 remains elusive. Our data suggest that the localized photothermal heating following LSPR  
68 excitation plays an important role toward favoring the reaction step involving product desorption  
69 from the biocatalytic active sites, ultimately leading to increased reaction rates.

## 70 RESULTS AND DISCUSSION

71 The first step toward this study comprised CALB adsorption onto Au NPs. It is well  
72 established that enzymes can interact with Au NPs surfaces via the interaction of carboxyl and  
73 amine groups present in the amino acid residues of the enzyme structure, following a kinetic  
74 process that involves anchoring, crawling, and subsequent binding onto the NPs surface.<sup>24, 27, 28</sup> It  
75 has also been reported that electrostatic binding can take place between remaining carboxyl groups  
76 on the Au NPs' surface (*e.g.* from citrate employed during synthesis) and amino groups (*e.g.* Lys  
77 and Arg) from the enzyme structure.<sup>29</sup> Furthermore, enzymes containing thiolated amino acid  
78 residues may interact with the Au NPs surface by chemisorption.<sup>30, 31</sup> CALB presents ten thiolated  
79 residues in its structure, of which four are methionine and six are cysteine residues, forming three  
80 disulfide bonds<sup>32</sup> and providing favorable conditions<sup>32</sup> for anchoring enzymes onto the NPs  
81 surface.<sup>27</sup>

82 AuNSt were synthesized by a seed-mediated growth method,<sup>33, 34</sup> using ascorbic acid as  
83 reducing agent, silver nitrate to assist the growth of spiky nanostructures, and CALB as stabilizing  
84 molecule. AuNSp were synthesized according to the Turkevich method<sup>35</sup> and subsequently coated  
85 by CALB. Both AuNSt and AuNSp were washed by centrifugation and removal of the supernatant  
86 to ensure that only CALB molecules adsorbed onto the NPs surface. AuNSt and AuNSp showed  
87 great colloidal stability upon CALB adsorption. The corresponding nanobioconjugates are referred  
88 to as AuNSt@CALB and AuNSp@CALB, respectively. Figure 1A-D shows representative TEM  
89 images AuNSp@CALB (Figure 1A and B) and AuNSt@CALB (Figure 1C and D). Nanoparticle  
90 size distribution histograms are presented in Figure S1. The images confirm the formation of Au  
91 nanospheres and nanostars with spiky morphology and sharp tips branching out from a central  
92 core. Both AuNSt@CALB and AuNSp@CALB displayed a relatively narrow size distribution,  
93 with diameters corresponding to  $12 \pm 2$  and  $100 \pm 20$  nm, respectively. For AuNSt, the tip  
94 dimensions were approximately  $45 \pm 5$  nm in length and  $5 \pm 0.6$  nm in width. Although not  
95 conclusive, high-resolution TEM images (Figure 1B and D) evidenced the presence of an organic  
96 layer on AuNSp and AuNSt surfaces, which may correspond to adsorbed CALB. The  
97 morphologies of AuNSp and AuNSt were thus preserved upon CALB adsorption and no  
98 aggregation was observed, even after laser irradiation (Figure S2). This indicates that CALB  
99 served as a suitable stabilizing agent for both AuNSp and AuNSt. AuNSp@CALB and  
100 AuNSt@CALB exhibited intense LSPR bands around 525 nm and 700 nm, respectively (Figure  
101 1E). These LSPR band positions were exploited to study the effect of on and off resonance  
102 conditions, relative to the NIR laser wavelength employed in CALB biocatalysis studies (808 nm,  
103 indicated by the dashed line in Figure 1E).

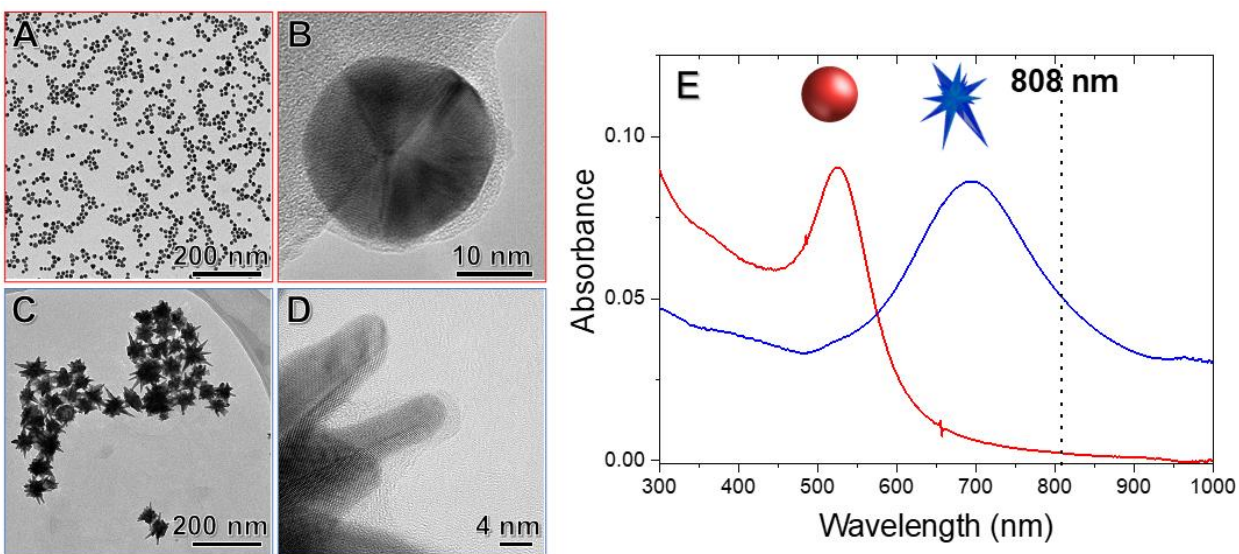


**Figure 1.** (A-D) TEM (A and C) and high resolution TEM (B and D) images of AuNSp@CALB (A and B) and AuNSt@CALB (C and D). (E) UV-Vis extinction spectra registered from aqueous suspensions containing of AuNSp@CALB (red trace) and AuNSt@CALB (blue trace). The 808 nm wavelength employed for biocatalysis studies is indicated by the black dashed line.

104

105 We then turned our attention to the study of CALB activity toward the hydrolysis of 4-  
 106 nitrophenyl palmitate (*p*NPP) as a model reaction (see Scheme 1 in the Experimental section). We  
 107 found that CALB activity (under light off conditions) decreased upon its adsorption on both AuNSt  
 108 and AuNSp (Table 1). This behavior is a common trend typically observed for immobilized  
 109 enzymes, being established that external mass transport restrictions limit their activity.<sup>36</sup> We  
 110 determined the catalytic rate constant ( $k_{\text{cat}}$ ), the binding Michaelis constant ( $K_M$ ), and the catalytic  
 111 efficiency ( $k_{\text{cat}}/K_M$ ) of free CALB and the same apparent parameters for the adsorbed enzyme  
 112 (Table 1 and Figure S3). Under light off conditions, the decrease in  $k_{\text{cat}}$  values for CALB adsorbed  
 113 on the Au NPs can be related to a partial loss of enzyme activity. Nevertheless, the  $K_M$  values of  
 114 adsorbed enzymes on the Au NPs were significantly smaller as compared to free CALB. This  
 115 lower apparent  $K_M$  suggests an increase of substrate local concentration at the NP surface, which  
 116 causes the higher activities observed at lower bulk substrate concentration. This effect was more

117 evident for AuNSt than for AuNSp. Similar results were obtained with a homologous lipase from  
 118 *Candida rugosa* immobilized on AuNSp.<sup>26</sup> The  $k_{cat}/K_M$  value decreased upon CALB adsorption  
 119 on the Au NPs, but that decay was 1.7 times lower for AuNSt@CALB than for AuNSp@CALB.  
 120 The different kinetic behavior of CALB on the two different NP morphologies can be related to  
 121 the enzyme density for nanoparticles with different curvature, where NPs with a smaller size (*i.e.*,  
 122 with a higher curvature) display a higher enzyme activity.<sup>23</sup> In this context, the tips of AuNSt (*ca.*  
 123 5 nm in diameter) can provide a surface of much higher curvature, compared to AuNSp (diameter  
 124 around 20 nm), leading to a lower density of CALB at the NP surface that results in a higher  
 125 enzyme activity.

126 **Table 1.** Kinetic parameters determined from Michaelis-Menten plots (Figure S3) for samples  
 127 under light on and off (dark) conditions <sup>a</sup>.

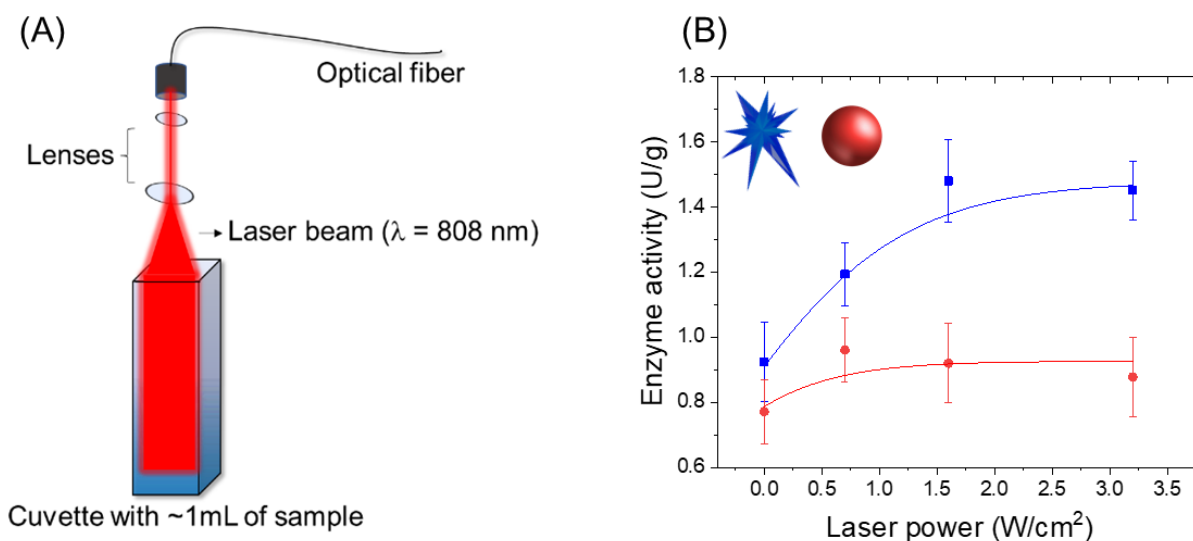
Sample	$k_{cat}$ (min <sup>-1</sup> )		$K_M$ (μM)		$k_{cat}/K_M$ (μM <sup>-1</sup> x min <sup>-1</sup> )	
	OFF	ON	OFF	ON	OFF	ON
AuNSt@CALB <sup>b</sup>	2461 ± 82	3947 ± 240	3.2 ± 0.4	5.1 ± 0.5	773 ± 180	765 ± 448
AuNSp@CALB <sup>c</sup>	2140 ± 126	2705 ± 372	4.8 ± 0.6	7.0 ± 2.0	443 ± 192	385 ± 186
Free CALB <sup>d</sup>	15855 ± 732	15966 ± 758	10.4 ± 4.3	9.7 ± 3.9	1520 ± 169	1640 ± 192

128 <sup>a</sup> Reaction conditions: PBS buffer at pH 7.4; at room temperature (approx. 20 °C); NIR laser irradiation at 3.2 W/cm<sup>2</sup>.  
 129 Enzyme concentration used: <sup>b</sup> 1.5 μmol L<sup>-1</sup>, <sup>c</sup> 1.0 μmol L<sup>-1</sup>, and <sup>d</sup> 1.1 μmol L<sup>-1</sup>. The kinetic constants calculated for the  
 130 immobilized enzymes are apparent constants, since they also account for mass transfer restrictions.

131

132 We further studied the effect of light irradiation on the hydrolytic activity of  
 133 AuNSt@CALB and AuNSp@CALB under different irradiation conditions. The reactions were  
 134 carried out in a quartz cuvette illuminated with a NIR laser at  $\lambda = 808$  nm, measuring the release

135 of 4-nitrophenolate (*p*NP) *in situ*, using a UV-Vis spectrophotometer (Figure 2A). Unlike the  
136 results under dark conditions, NIR irradiation enhanced the enzymatic activity of AuNSt@CALB  
137 to a significantly higher extent than that for AuNSp@CALB irradiated under the different laser  
138 powers (Figure 2B and Table 1). This result agrees with the better match between the incoming  
139 light wavelength (808 nm) and the LSPR position in AuNSt (700 nm, Figure 1E), as compared to  
140 AuNSp (525 nm, Figure 1E). In the case of AuNSt@CALB, the activity increases with laser power  
141 until reaching a plateau at laser powers above 1.6 W/cm<sup>2</sup>. No differences were observed for the  
142 activity of free CALB under light on and off conditions (Figure S4). Therefore, NIR irradiation  
143 only leads to a significant enhancement on the activity of CALB molecules at the surface of  
144 AuNSt, which feature a LSPR position which better matches the light excitation wavelength.



145  
146 **Figure 2.** (A) Schematic illustration of the laser irradiation setup. (B) Effect of NIR laser power  
147 ( $\lambda = 808$  nm) on the enzymatic activity of AuNSt@CALB (blue squares) and AuNSp@CALB (red  
148 circles).

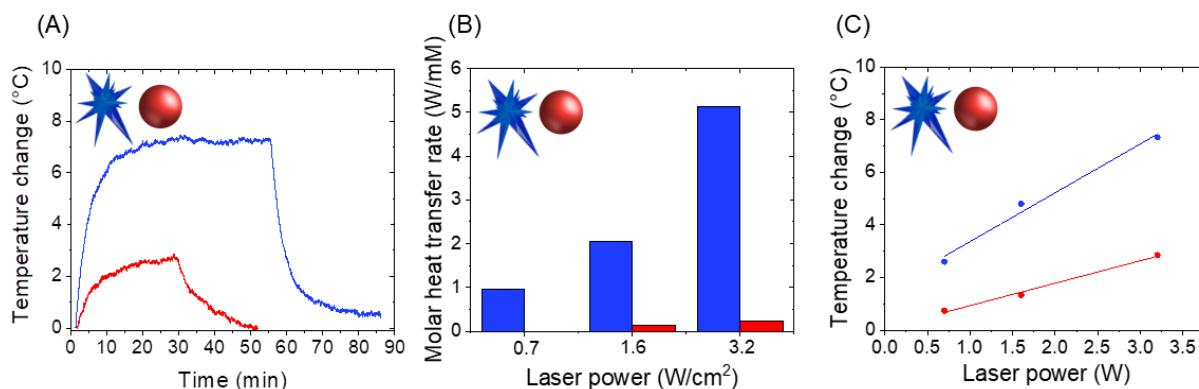
149  
150 To unravel the effect of LSPR excitation over enzymatic activity, we investigated the  
151 heating capacity of AuNSt and AuNSp under the employed light irradiation conditions. The  
152 samples were therefore illuminated with the NIR laser and the temperature changes in the colloidal



153 dispersion over time were monitored with a thermal camera. When the temperature reached  
154 thermal equilibrium, the laser was turned off and the cooling down curve was recorded to quantify  
155 heat dissipation to the solution. Figure 3A shows exemplary heating and cooling curves for both  
156 AuNSt@CALB and AuNSp@CALB. The molar heat transfer rates for both AuNSt and AuNSp  
157 were calculated by fitting these temperature time-courses to Equation 1,<sup>37</sup> as illustrated in Figure  
158 3B.

$$159 \quad \frac{\Delta Q}{c_{Au}} = \frac{Q_{sample} - Q_{medium}}{\epsilon_{400}/2.4 \text{ mmolL}^{-1}} \quad (1)$$

160 Here, the generated heat output ( $\Delta Q$ ), obtained from the heat difference between the sample  
161 ( $Q_{sample}$ ) and the medium ( $Q_{medium}$ ), is related in terms of the estimated gold concentration ( $c_{Au} =$   
162  $\epsilon_{400}/2.4 \text{ mmol L}^{-1}$ )<sup>38</sup> in the sample. It was found that the molar heat transfer rate was much larger  
163 for AuNSt@CALB than for AuNSp@CALB. In this case, LSPR excitation leads to photothermal  
164 heating because of plasmon decay. Such a photothermal heating effect takes place close to the  
165 NPs' surface and is further dissipated to the reaction mixture, leading to the detected temperature  
166 increase. Our data indicate that AuNSt are more efficient nano-sources of heat<sup>8</sup> than AuNSp under  
167 the employed NIR irradiation conditions. In fact, Figure 3C shows that AuNSt@CALB under NIR  
168 irradiation ( $3.2 \text{ W/cm}^2$ ) were capable to increase the bulk temperature of the reaction mixture up  
169 to  $7.3 \text{ }^\circ\text{C}$ , versus the  $2.7 \text{ }^\circ\text{C}$  observed for AuNSp@CALB under the same conditions. As expected  
170 from the photothermal heating triggered by LSPR excitation, we observed an increase of the bulk  
171 temperature by increasing the laser power.



172

173 **Figure 3.** Plasmonic heating effects of NIR laser ( $\lambda = 808$  nm) on AuNSt@CALB (blue) and  
 174 AuNSp@CALB (red). (A) Example of heating and cooling curves (laser power 3.2 W/cm<sup>2</sup>). (B)  
 175 Molar heat transfer rate vs. laser power. (C) Temperature changes measured in colloidal  
 176 dispersions of AuNSt@CALB (blue) and AuNSp@CALB (red).

177

178 In this context, it is expected that photothermal heating can lower the activation energy of  
 179 the enzyme, according to the Arrhenius analysis<sup>22</sup>, thereby leading to higher enzyme activity. This  
 180 effect was further confirmed by activity assays for both free CALB and adsorbed onto Au NPs,  
 181 under different temperatures, as shown in Figure 4A. Typically, each class of enzyme exhibits an  
 182 optimal temperature where the highest activity is observed.<sup>39</sup> Above this value, the activity  
 183 gradually decreases due to protein denaturation. Free CALB showed an optimal temperature of 55  
 184 °C (Figure 4A), in agreement with previously reported data.<sup>40</sup> At temperatures above 55 °C, free  
 185 CALB undergoes thermal deactivation and its activity decreases considerably. Conversely, the  
 186 enzymatic activity increased with temperature, even at values above 55 °C, for AuNSt@CALB  
 187 and AuNSp@CALB. The preservation of enzyme activity at high temperatures indicates that the  
 188 adsorption of CALB on Au NPs enhances the enzyme thermal stability. Circular dichroism (CD)  
 189 spectroscopy studies (Figure 4B and Figure S5) demonstrate the higher conformational stability of  
 190 enzymes adsorbed on both AuNSt and AuNSp, which explains their higher enzyme activities at  
 191 temperatures above 55 °C. The observed decrease in mean residue ellipticity (MRE) at 222 nm

192 corresponds to major conformational changes in the  $\alpha$ -helix secondary structure of CALB (Figure  
 193 4B). The adsorption of CALB on AuNSt precludes the structural distortions induced by the higher  
 194 temperatures, as no significant ellipticity changes were observed up to 48 °C. However, the  
 195 conformation of free CALB was gradually distorted at temperatures higher than 25 °C.

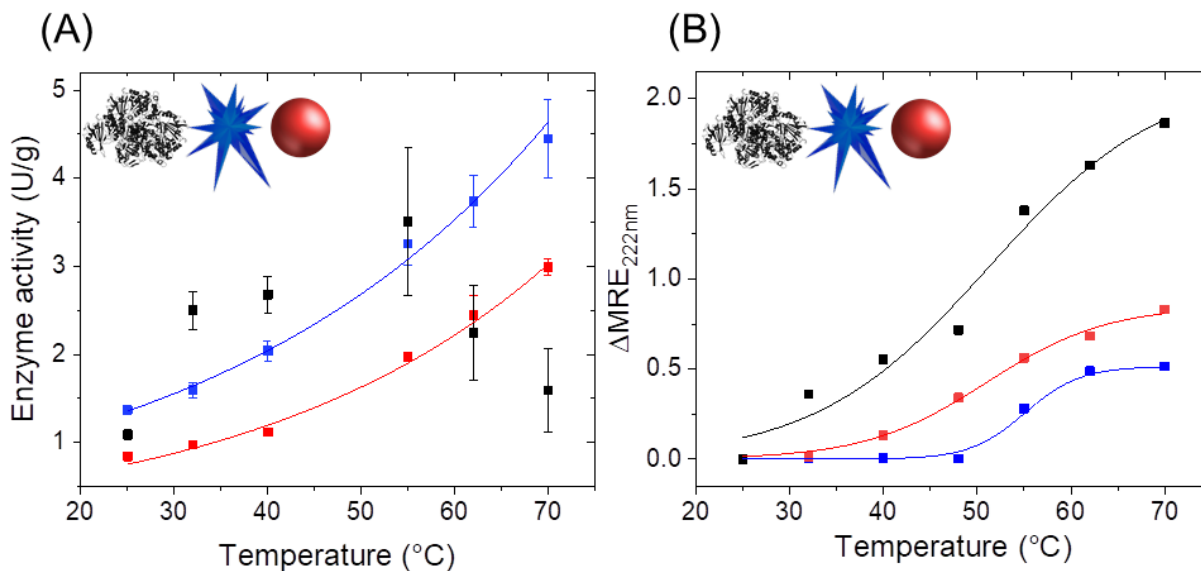


**Figure 4.** Temperature effects at dark conditions on enzymatic activity (A) and enzyme secondary structure (B), for AuNSt@CALB (blue), AuNSp@CALB (red), and free CALB (black). (A) Enzymatic activity as a function of temperature, fitted to the Arrhenius model. (B) Thermal denaturation of the enzyme conformation monitored by the variation of MRE ( $\Delta MRE = MRE_{25^\circ C} - MRE_T$ ) at 222 nm, measured by CD spectroscopy. CD data were obtained by an average of 10 accumulation spectra for each sample.

196

197 Interestingly, the activity vs. temperature correlation (Figure 4A) serves as a calibration  
 198 curve for the indirect evaluation of local gradients occurring under irradiation conditions (Figure  
 199 2B). This strategy has been previously used to determine the local heating of magnetic iron oxide  
 200 nanoparticles under alternating magnetic fields.<sup>41</sup> As presented in Figure 2B, the enzymatic  
 201 activity of AuNSt@CALB under 3.2 W/cm<sup>2</sup> laser irradiation was 58% higher than that under non-  
 202 irradiated conditions at the same bulk temperature (room temperature). We know that the particles

203 under  $3.2 \text{ W/cm}^2$  laser irradiation are only capable to heat the bulk up to  $32 \text{ }^\circ\text{C}$  (Figure 3C).  
204 However, a proportional activity enhancement of 58% would correspond to a bulk temperature of  
205 roughly  $42 \text{ }^\circ\text{C}$  (see Figure 4A). The differences between the expected activity according to the bulk  
206 temperature correlation (Figure 4A) and the measured activity under laser irradiation (Figure 2B)  
207 suggest the existence of a local temperature gradient between the AuNSt surface and the bulk. In  
208 this way, according to the obtained enzyme activity values, we can estimate a  $10 \text{ }^\circ\text{C}$  gradient  
209 difference between the enzyme environment ( $42 \text{ }^\circ\text{C}$ ) and the bulk ( $32 \text{ }^\circ\text{C}$ ). This observation may  
210 also be related to previous studies describing the inactivation of enzymes immobilized on Au NPs  
211 under laser irradiation, likely due to an excess of local heating.<sup>10,11</sup>

212 Previous studies have described similar observations on the thermal effects promoted by  
213 light absorption.<sup>10-15</sup> Recently, the effects of photothermal heating and LSPR excited charge  
214 carriers were investigated in plasmonic catalysis,<sup>4,8,9</sup> but a clear distinction of their contributions  
215 remains challenging. This is because photothermal heating is largely unavoidable following LSPR  
216 excitation.<sup>42</sup> In the present case, AuNSt seem to release more photothermal heating to the  
217 surrounding media as a result of a more efficient LSPR excitation<sup>8, 43</sup> leading to a larger  
218 enhancement in the enzyme activity. Moreover, it is plausible that water pocket interfaces present  
219 in the enzyme structure can result in higher yields of energy distribution throughout the enzyme  
220 structure.<sup>44</sup> Lastly, we argue that discussing the activity enhancement mechanism through a  
221 mechanism based on LSPR-excited charge carriers would be too speculative, as the hydrolysis  
222 mechanism does not involve electron transfer and CALB lacks any metallic center that may  
223 facilitate electron shuttle. Although both mechanisms might occur simultaneously, electronic  
224 effects can be hardly assessed for this system using state-of-the-art methodologies, whereas  
225 photothermal effects are more accessible as we showed.

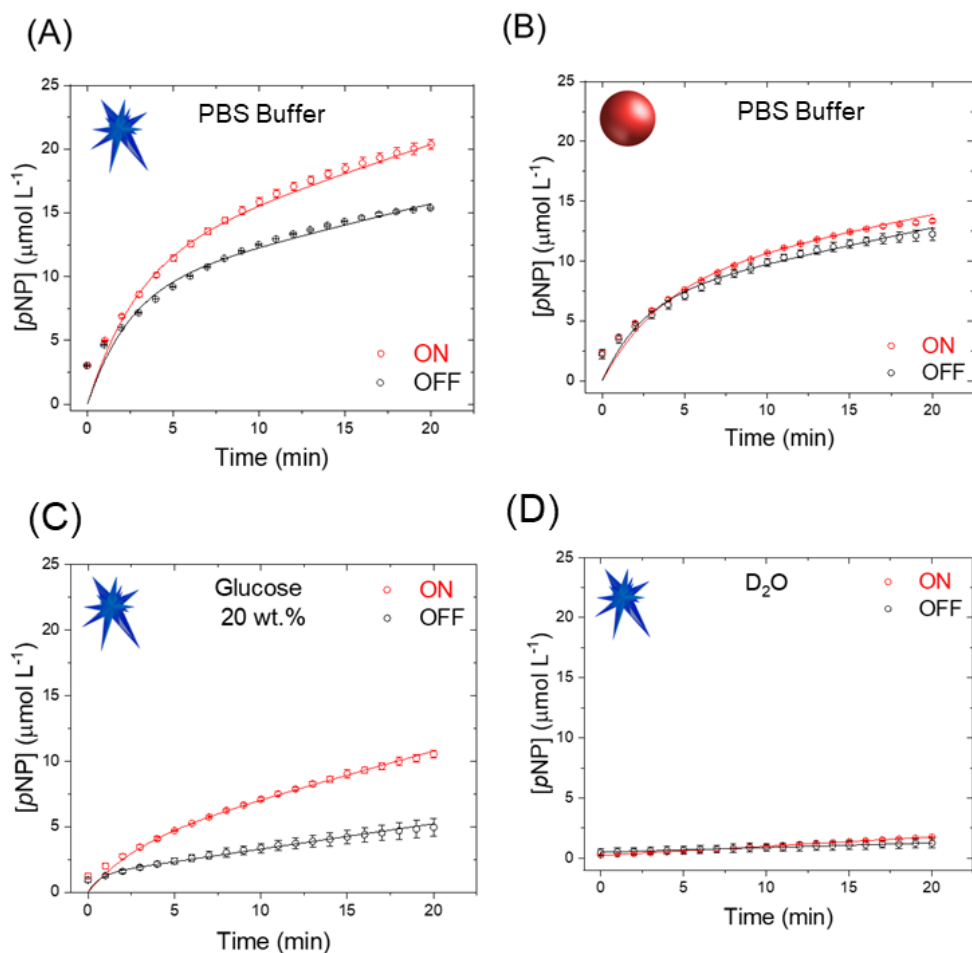
226 Inspired by these results, we performed a series of studies to understand the effect of LSPR  
227 excitation on the activity enhancement observed for AuNSt@CALB through determination of the  
228 steady-state kinetic parameters under irradiation conditions. First of all, we investigated how the  
229 maximum reaction rate and  $k_{\text{cat}}$  were affected by light irradiation when CALB was adsorbed on  
230 Au NPs (Table 1 and Figure S3). The value of the apparent  $k_{\text{cat}}$  is 60% higher for AuNSt@CALB  
231 under irradiation than under non-irradiation conditions. This effect was less noticeable for  
232 AuNSp@CALB, and even less for free CALB. Interestingly,  $K_M$  values increased under laser  
233 irradiation only when CALB was adsorbed on Au NPs, with no apparent changes in free CALB,  
234 suggesting that laser irradiation influences the enzymatic activity when CALB is at the Au NPs  
235 surface. The  $k_{\text{cat}}/K_M$  showed similar values for all samples, regardless of light irradiation, because  
236 the effect of light on the catalytic constant is compensated by the effect on the binding constant.  
237 The higher  $k_{\text{cat}}$  values under irradiation conditions are probably due to the higher local temperature  
238 at the surface of AuNSt, which is also supported by the analysis based on Arrhenius plots (Figure  
239 S6). The activation energy barrier for the enzyme activity on AuNSt@CALB decreased from 32  
240 to 21 kJ mol<sup>-1</sup> when the laser was turned on. In contrast, light was unable to alter the activation  
241 energy of the free enzyme, supporting that the interface between the enzyme and AuNSt played a  
242 key role to enhance the enzymatic activity through plasmonic effects.

243 We next performed a more detailed analysis of the reaction time-courses that revealed  
244 fundamental mechanistic information for the performance of CALB adsorbed on Au NPs, under  
245 light irradiation conditions (Figure 5). According to the general enzymatic mechanism (see Figure  
246 6), the reaction kinetics are driven by an initial fast equilibrium binding step followed by an  
247 irreversible chemical step. Assuming that the second step of the lipase reaction is the rate-limiting  
248 one, the activity assay we used does not account for the product release of the acid,<sup>28, 45, 46</sup> since

249 the colorimetric method only detects the product *p*NP. The reaction time-courses in Figure 5 were  
250 fitted to the initial-burst kinetic model as described by Equation 2, to better estimate the second  
251 step of the lipase mechanism.<sup>47</sup>

$$252 \quad [P] = vt + [E_0] * (1 - e^{-k_{obs}t}) \quad (2)$$

253 Here, the concentration of the formed product (P) is related to the initial velocity (*v*), the initial  
254 concentration of the enzyme (*E*<sub>0</sub>), and the rate constant (*k*<sub>obs</sub>), as a function of time (*t*) (see Figure  
255 S7). In this kinetic model, if *k*<sub>obs</sub> >> *v*, *v* accounts for the rate-limiting step in the enzymatic  
256 mechanism of CALB, which we assign to the steps of hydrolysis of the acyl-enzyme complex and  
257 product release. Looking beyond the initial burst in the early stages of product conversion with  
258 AuNSt@CALB, Figure 5A illustrates that light irradiation affects more significantly the second  
259 phase (after ca. 5 min) of the time-courses. Indeed, AuNSt@CALB exhibited a *v* value which is  
260 36% higher under irradiation than under non-irradiation (dark) conditions. Such a light-driven  
261 enhancement was higher than that observed for AuNSp@CALB (12%). The time-course  
262 conversion as a function of time for free CALB did not fit this kinetic model, but the Michaelis-  
263 Menten kinetic parameters clearly demonstrate that the activity of the free enzyme was not affected  
264 by light irradiation. Consequently, laser irradiation appears to play a relevant role in the rate-  
265 limiting step of the enzyme reaction mechanism.



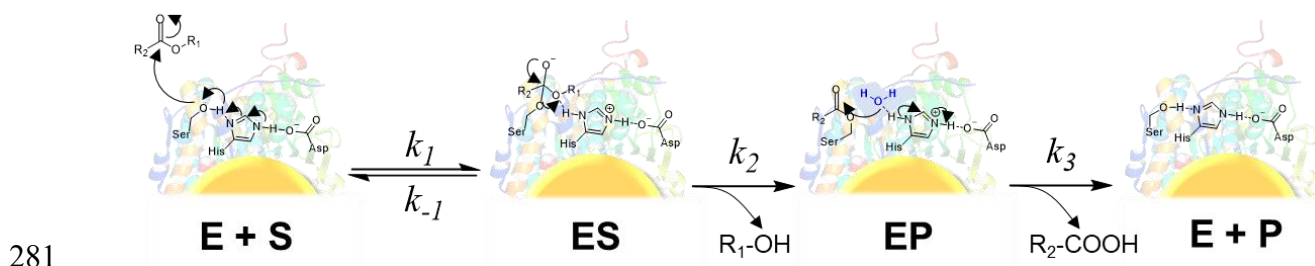
266

267 **Figure 5.** Time-courses of pNPP hydrolysis catalyzed in PBS buffer (A and B) by AuNSt@CALB  
 268 (A, C and D) and AuNSp@CALB (B), under NIR irradiation ( $3.2 \text{ W/cm}^2$ ) and non-irradiation  
 269 (dark) conditions. Viscosity (C) and solvent isotopic (D) effects on the time dependence of the  
 270 product formation for AuNSt@CALB. Viscosity assays were performed in presence of glucose 20  
 271 wt.% and solvent isotopic assays were performed in the presence of  $\text{D}_2\text{O}$ . All experimental data  
 272 were fitted to an initial-burst kinetic model (Equation 2) and the respective values are listed in  
 273 Table S1.

274

275 To explain the effect of light on CALB activity from a mechanistic point of view, we  
 276 inspected the well-known three-step catalytic mechanism of hydrolases (Figure 6).<sup>23, 26, 45, 48, 49</sup>  
 277 This mechanism is defined by four distinct rate constants ( $k_1$ ,  $k_{-1}$ ,  $k_2$ ,  $k_3$ ).<sup>26, 45, 49</sup> Therefore, to  
 278 decipher whether light affects either chemical hydrolysis, product release or both steps, reaction

279 time-courses were recorded with AuNSt@CALB in different reaction media, under both light and  
280 dark conditions.



282 **Figure 6.** Scheme of the general mechanism for a lipase catalytic reaction. The constants  $k_1$  and  
283  $k_{-1}$  are related to reversible binding of the substrate (S) to the enzyme (E) active site, to form the  
284 transient intermediate (ES);  $k_2$  rules the formation of the acyl-enzyme complex and release of the  
285 alcohol product (EP);  $k_3$  accounts for the hydrolysis of that complex, releasing the acid product to  
286 the bulk (E +P).

287

288 We first monitored reaction time-courses in viscous media (20 wt% glucose), aiming at  
289 hampering the product diffusion out the active center (state E+P). The interchain hydrogen bonds  
290 formed between glucose molecules increase the medium viscosity<sup>50</sup>, like other sugar solutions  
291 such as sucrose,<sup>22, 23</sup> which is known to hamper product release from the enzyme  
292 microenvironment. Under these conditions, the product release appears to be the dominant rate-  
293 limiting step,<sup>23, 48</sup> so the effects of laser irradiation on the  $\nu$  parameter of the initial-burst model  
294 compared to the corresponding control experiments (no glucose) can be quantified. Under both on  
295 and off conditions, more viscous reaction media slowed down product formation along time  
296 (Figure 5C and Table S1). Remarkably, light irradiation significantly accelerated (by 40%) the  
297 slowest phase of the time-courses using AuNSt@CALB under viscous conditions. Conversely, the  
298 influence of light on the performance of both AuNSp@CALB and free CALB was negligible  
299 (Figure S8). To confirm the results extracted from the burst-kinetic model, and considering the



300 deacylation of the enzyme as the slower step (*i.e.*,  $k_3 \ll k_2$ ), which means that  $k_3$  is the rate-limiting  
301 step (*i.e.*,  $k_{cat} = k_3$ ) as supported by recent computational studies<sup>51</sup>, we constructed the three-step  
302 kinetic model showed in Figure 6 using the software COPASI.<sup>52</sup> This model allowed us to estimate  
303  $k_3$  values from the reaction courses obtained with AuNSt@CALB (see Table S2 and Figure S9).  
304 We found that  $k_3$  follows the same trend as the  $v$  parameter calculated from the initial-burst kinetic  
305 model. Light increases by 2-fold the  $k_3$  value of AuNSt@CALB, compared to the non-irradiated  
306 reaction, and the  $k_{3(ON)}/k_{3(OFF)}$  ratio is maximized under viscous reaction media (in the presence of  
307 glucose) by a factor of 3.5 (Figure S10). These experimental results suggest that light contributes  
308 to enhancing the catalytic properties of AuNSt@CALB through easing the product release (state  
309 E+P) from enzyme close to the plasmonic NPs surface. Subsequently, to evaluate whether light  
310 can also affect the kinetics of the hydrolytic step (state EP), the kinetic isotopic effect (KIE)<sup>53</sup> was  
311 studied by using heavy water ( $D_2O$ ) under laser on and off conditions, and the results were  
312 compared to their corresponding control experiments (in  $H_2O$ ). In this step, water molecules from  
313 the medium play a crucial role in the nucleophilic attack for cleaving the carbonyl group bond of  
314 the acyl-enzyme complex.<sup>26, 49</sup> When using  $D_2O$  as solvent, the enzyme activity dramatically  
315 decreased for both conditions, as expected from the occurrence of an isotopic effect in the  
316 hydrolysis step<sup>53</sup> (Figure 5D). Hence, we observe a KIE of  $v(H_2O)/v(D_2O)$  of 8.67, which  
317 demonstrates that the hydrolysis of the acyl-enzyme complex dominates the rate-limiting step ( $k_3$ ).  
318 On the other hand, when the reaction time-courses were recorded in the presence of  $D_2O$  and under  
319 irradiation conditions, light had a negligible effect on the enzymatic rates. Hence, when the  
320 hydrolysis of the acyl-enzyme complex is extremely slow due to isotopic effects, NIR laser  
321 irradiation no longer affects the rate-limiting step of the AuNSt@CALB catalysis mechanism.  
322 Interestingly, these results indicate that plasmonic excitation hardly affects the kinetics of water

323 attack, while it significantly increases the efficiency of the product release step. When compared  
324 to the activity of soluble CALB measured in PBS buffer, we found a stronger temperature  
325 dependence of the free enzyme activity in viscous media, but a weaker dependence in D<sub>2</sub>O. These  
326 results further support the enhancement of product release when the enzyme is locally heated at the  
327 interface with the irradiated plasmonic nanoparticle (Figure S11). Previous studies reporting that  
328 enzyme immobilization on the surface of nanoparticles leads to more significant changes in the  
329 product release step in the enzymatic kinetics<sup>22, 23</sup> also support the assumption that the major  
330 contribution of light is related to this step. Therefore, our results demonstrate that LSPR excitation  
331 increases the activity of AuNSt@CALB by enhancing the kinetics of product release in the last  
332 step of the enzyme mechanism driven by  $k_3$ , as summarized in Figure 6. This effect has been  
333 observed exclusively with AuNSt@CALB, confirming that the LSPR of Au NPs must be in  
334 resonance with the incident NIR laser wavelength (808 nm), to exert the effect on enzyme  
335 properties.

## 336 CONCLUSION

337 We used CALB adsorbed on the surface of Au nanospheres (NSp) and nanostars (NSt) as  
338 a model system to unravel the effect of light illumination, and thus LSPR excitation, on the  
339 underlying mechanisms behind the plasmonic enhancement of enzyme activity under NIR  
340 excitation. It was found that LSPR excitation in the NIR enabled an increase of 58% in enzyme  
341 activity when Au NSt were employed as immobilization carriers. In addition to the enhanced  
342 activities, we investigated the effect of plasmonic excitation on the rate-limiting step of the  
343 enzymatic reaction. Data from highly viscous conditions and solvent isotopic effects revealed that  
344 photothermal heating from LSPR excitation accelerated the latest step of the reaction by favoring  
345 product release, rather than improving the hydrolytic step at the interface between the enzyme and

346 the plasmonic NPs. We envision that some of the mechanistic conclusion reached in this work can  
347 be translated to other combinations of enzymes and plasmonic NPs, and may inspire the rational  
348 design of plasmonic NPs and enzyme hybrids with target activities and selectivity that can be  
349 externally controlled by light excitation.

## 350 EXPERIMENTAL SECTION

351 **Materials.** Lipase from *Candida antarctica* fraction B (CALB), tetrachloroauric acid  
352 ( $\text{HAuCl}_4 \cdot 3\text{H}_2\text{O}$ ), sodium citrate tribasic dihydrate, ascorbic acid, silver nitrate, 4-nitrophenyl  
353 palmitate were purchased from Sigma-Aldrich. Phosphate-buffered saline was purchased from  
354 Biochrom GmbH, (Berlin, Germany). CALB solutions were prepared in PBS buffer pH 7.4. The  
355 concentration of CALB was determined by the colorimetric kit Bradford assay<sup>54</sup>, purchased from  
356 Thermo Scientific. All chemicals were used as received. Purified Milli-Q water (Millipore, 18.2  
357  $\text{M}\Omega \text{ cm}$ ) was used in the preparation of all solutions.

### 358 **Gold nanoparticles synthesis and CALB adsorption.**

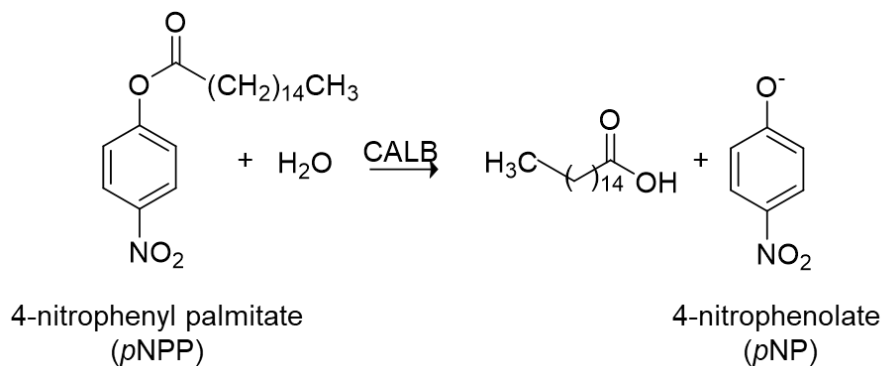
359 *AuNSp@CALB synthesis.* AuNSp were obtained by Turkevich method.<sup>55</sup> In a typical procedure,  
360 150 mL of  $2.2 \text{ mmol L}^{-1}$  sodium citrate solution under vigorous stirring was heated until boiling.  
361 Then, 1 mL of  $25 \text{ mmol L}^{-1}$   $\text{HAuCl}_4 \cdot 3\text{H}_2\text{O}$  was added. The temperature was decreased to  $\sim 90 \text{ }^\circ\text{C}$   
362 and the solution color change from soft yellow to red in  $\sim 10$  min. After the solution reach  $90 \text{ }^\circ\text{C}$ ,  
363 1 mL of  $60 \text{ mmol L}^{-1}$  sodium citrate solution and 1 mL of  $25 \text{ mmol L}^{-1}$   $\text{HAuCl}_4 \cdot 3\text{H}_2\text{O}$  were  
364 subsequently added, and let it stir during 30 min at  $90 \text{ }^\circ\text{C}$ . After cooling to room temperature,  
365 samples were stored in fridge for further use. The adsorption of CALB onto AuNSp to obtain  
366 AuNSp@CALB bioconjugates was adapted from a previously described method.<sup>24</sup> First,  $0.1 \text{ mg}$   
367  $\text{mL}^{-1}$  CALB stock solutions were prepared in PBS buffer pH 7.4. 10 mL of CALB solution was

368 added to 10 mL of previously synthesized AuNSp. The sample was incubated during 2h at 32 °C  
369 and 300 rpm in an Eppendorf thermomixer. After, before using, the colloidal dispersion was  
370 washed by centrifugation at 13 000 rpm during 20 min to remove the excess of CALB and possible  
371 non-reactants from AuNSp synthesis. The precipitate was washed and re-dispersed in PBS buffer.  
372 Samples were previous analyzed by UV-Vis spectroscopy (Agilent 8453) to monitor the LSPR  
373 signal and to determine the molar gold concentration in the samples at  $\lambda = 400 \text{ nm}^{38}$ .  
374 AuNSp@CALB final concentration of Au was  $0.84 \mu\text{mol L}^{-1}$  and of CALB was  $1.06 \mu\text{mol L}^{-1}$ .

375 *AuNSp@CALB synthesis.* AuNSp@CALB synthesis were adapted from a previously described  
376 method.<sup>33, 34</sup> AuNSp were obtained by seed-mediated growth. Firstly, seed solution was prepared  
377 by adding 5 mL of  $34 \text{ mmol L}^{-1}$  sodium citrate into 95 mL of  $0.5 \text{ mmol L}^{-1}$   $\text{HAuCl}_4 \cdot 3\text{H}_2\text{O}$  under  
378 boiling and vigorous stirring, and it was let stirring during 15 min at the same temperature and  
379 stirring. After cooling to room temperature, the colloidal dispersion was stored in fridge for further  
380 use. For AuNSp synthesis, 100  $\mu\text{L}$  of  $25 \text{ mmol L}^{-1}$   $\text{HAuCl}_4 \cdot 3\text{H}_2\text{O}$  was added into 10 mL of  $\text{H}_2\text{O}$   
381 containing 10  $\mu\text{L}$  of  $1 \text{ mmol L}^{-1}$  HCl under vigorous stirring at room temperature. Then, 100  $\mu\text{L}$   
382 of seed solution, 100  $\mu\text{L}$  of  $3 \text{ mmol L}^{-1}$  silver nitrate solution and 50  $\mu\text{L}$  of  $100 \text{ mmol L}^{-1}$  ascorbic  
383 acid solution were quickly subsequent added. After 3-5 min of stirring, 10 mL of  $0.1 \text{ mg mL}^{-1}$   
384 CALB solution was added and let it stirring for 5 min. Then, the sample was stored in fridge for  
385 further use. Samples were washed just before the use by centrifugation at 7000 rpm during 15 min  
386 to remove the excess of CALB and possible non-reactants from AuNSp synthesis. The precipitate  
387 was washed and re-dispersed in PBS buffer. Samples were previous analyzed by UV-Vis  
388 spectroscopy (Agilent 8453) to monitor the LSPR signal and to determine the molar gold  
389 concentration in the samples at  $\lambda = 400 \text{ nm}^{38}$ . AuNSp@CALB final concentration of Au was  $0.54$   
390  $\mu\text{mol L}^{-1}$  and of CALB was  $1.14 \mu\text{mol L}^{-1}$ .

391 **Enzymatic activity assays.**

392 *pNPP hydrolysis time dependence of the product formation.* Enzymatic activity of free CALB and  
393 CALB-AuNSp bioconjugates were determined by measuring the release of 4-nitrophenolate (*p*NP)  
394 from the hydrolysis of 4-nitrophenyl palmitate (*p*NPP) (Scheme 1), monitored by UV-Vis  
395 spectroscopy at  $\lambda = 405$  nm, as previously described elsewhere.<sup>24, 26</sup> In a quartz cuvette containing  
396 1000  $\mu$ L of PBS buffer pH 7.4, 36  $\mu$ L of 0.5 mmol L<sup>-1</sup> *p*NPP solution previously prepared in  
397 isopropanol was added. All *p*NPP solutions were prepared in the same day before use.  
398 Subsequently, 36  $\mu$ L of the sample was added and homogenized. The solution change slowly from  
399 transparent to light yellow upon *p*NP release, according to the amount of CALB in the sample.  
400 *p*NP concentration was determined from Lambert-Beer's law using molar extinction coefficient of  
401  $\epsilon = 12800$  mol L<sup>-1</sup> cm<sup>-1</sup>.<sup>26</sup> The enzymatic activity was determined from the initial velocity obtained  
402 from the linear slope of *p*NP concentration versus time plot. The unit U/g corresponds to 1  $\mu$ mol  
403 of the product *p*NP formed per 1 min of reaction related to the amount of protein. For the assays  
404 upon laser illumination, the cuvette was illuminated vertically (see illustrative scheme in Figure  
405 2A) and measures of the absorbance of *p*NP formation were recorded at each 1 min during  
406 approximately 20 min.



407

408 **Scheme 1.** Hydrolysis of pNPP biocatalyzed by CALB. The reaction rate can be monitored from  
 409 pNP formation, by monitoring absorbance at  $\lambda = 405$  nm.

410

411 *Michaelis-Menten.* Enzymatic kinetics of free CALB and CALB-AuNPs bioconjugates were  
 412 determined by the typical procedure of Michaelis-Menten model<sup>28, 56</sup>. First, pNPP solutions at  
 413 initial concentrations of 0.5, 0.4, 0.3, 0.2, 0.1, 0.05, and 0.01 mmol L<sup>-1</sup> were prepared in  
 414 isopropanol. All pNPP solutions were prepared at the same day before use. The same procedure  
 415 described in the previous topic for pNPP hydrolysis time dependence of the product formation to  
 416 determine the enzyme activity was performed. The values of the parameters maximum velocity  
 417 ( $V_{max}$ ) and Michaelis-Menten constant ( $K_M$ ), related to the initial velocity ( $V_o$ ) and substrate  
 418 concentration ( $[S]$ ), were obtained from the typical relation:

419 
$$V_o = \frac{V_{max} * [S]}{K_M + [S]} \quad (3)$$

420 *Arrhenius.* Arrhenius analysis was performed to determine the enzyme activation energy of free  
 421 CALB and CALB-AuNPs bioconjugates as described previously elsewhere<sup>22</sup>. The enzyme activity  
 422 was determined by the same procedure described in the former topic for pNPP hydrolysis, varying  
 423 the temperature from 25 to 80 °C. The values of activation energy ( $E_a$ ) were obtained from the  
 424 linear fitting from the relation described as

425 
$$\ln K = \ln A - \frac{E_a}{RT} \quad (4)$$

426 where, k is the rate constant, A is the pre-exponential factor, R is the universal gas constant at the  
427 absolute temperature (T).

428 *Viscosity and solvent isotope dependence.* Viscosity and solvent isotope dependence kinetics were  
429 performed as previous described elsewhere.<sup>23, 48</sup> For the viscosity assays, kinetics was performed  
430 in presence of 20 wt% glucose prepared in PBS buffer. For the solvent isotope assays, kinetics was  
431 performed in presence of D<sub>2</sub>O and all samples were previously washed and re-suspended in D<sub>2</sub>O  
432 to avoid any water molecules at the kinetics. Enzyme activity was determined by the same  
433 procedure described in the previous topic for pNPP hydrolysis time dependence of the product  
434 formation. Data were analyzed and fitted by an initial-burst of product kinetics model.<sup>47</sup>

435 **Heating experiments.** 1 mL of sample in a quartz cuvette was illuminated by a near-infrared laser  
436 at  $\lambda = 808$  nm (fiber-coupled laser diode, Lumics LU0808T040) laterally, passing through two  
437 lenses, one to collimate and other to expand the laser beam in order to illuminate a spot of 1 cm<sup>2</sup>  
438 onto the sample. The laser was illuminated upon different powers (0.7, 1.6, and 3.2 W/cm<sup>2</sup>) and  
439 monitored by using a thermal camera (FLIR A35) above the cuvette. The heating and cooling  
440 curves were obtained from the thermal camera data by using the ResearchIR software. PBS buffer  
441 and water were measured as blank curves to eliminate any contribution from the medium. The  
442 molar heat rate transfer was calculated by the relation<sup>37</sup>:

443 
$$\frac{\Delta Q}{c_{Au}} = \frac{Q_{sample} - Q_{medium}}{\epsilon_{400}/2.4 \text{ mmolL}^{-1}} \quad (5)$$

444 where, the generated heat output ( $\Delta Q$ ), obtained from the difference of heat from the sample  
445 ( $Q_{\text{sample}}$ ) and from the medium ( $Q_{\text{medium}}$ ), is related in terms of the estimate gold concentration ( $c_{\text{Au}}$   
446  $= \varepsilon_{400}/2.4 \text{ mmol L}^{-1}$ )<sup>38</sup> in the sample.

#### 447 **Characterization techniques.**

448 *Transmission electron microscopy (TEM).* TEM images were obtained by using a JEOL  
449 microscope at an acceleration voltage of 200 kV. Approximately 3  $\mu\text{L}$  of sample was dropped on  
450 a lacey carbon-coated grid and left to dry. The size distribution of nanoparticles obtained were  
451 analyzed by using ImageJ software.

452 *Circular dichroism (CD) spectroscopy.* CD measurements were obtained in a Jasco J-815 CD  
453 spectrometer. CD spectra were recorded in the range 200-260 nm, using a quartz cuvette of 5 mm,  
454 bandwidth of 5 nm, data pitch of 1 nm, scanning speed at 50 nm/min. The spectra were obtained  
455 by an average of 10 accumulations and corrected by the PBS buffer spectrum. The measurements  
456 were showed in molar residue ellipticity (MRE) by using the relation:

$$457 \quad MRE = \frac{MRW \times \theta}{10dc} \quad (6)$$

458 where, the measured ellipticity ( $\theta$ ) in degrees is related to the cuvette path length (d) in centimeters  
459 and the protein concentration (C) in  $\text{g mL}^{-1}$ . MRW corresponds to the mean residue weight defined  
460 by  $MRW = M / (N-1)$ , where M is the molecular mass in Daltons and N is the number of amino  
461 acids in the protein structure. For CALB,  $M = 33000 \text{ g mol}^{-1}$  and  $N = 317$ .<sup>40</sup>

462

463 ASSOCIATED CONTENT



464 **Supporting Information.**

465 The following files are available free of charge.

466 Additional information of LSPR characterization before and after NIR laser irradiation; Michaelis-  
467 Menten plots; NIR laser power effect on free CALB; CD spectra as function of temperature;  
468 Arrhenius plots, example of initial-burst of product kinetics; viscosity on time dependence of the  
469 product formation; fitting data carried out with COPASI and the values obtained; Table containing  
470 parameters obtained from kinetics fitted data and from COPASI software (PDF)

471 **AUTHOR INFORMATION**

472 **Corresponding Author**

473 Heloise R. Barros - Department of Fundamental Chemistry, Institute of Chemistry, University of  
474 São Paulo, Av. Prof. Lineu Prestes, 748, Vila Universitária, 05508-000 São Paulo, SP, Brazil; CIC  
475 biomaGUNE, Basque Research and Technology Alliance (BRTA), Paseo de Miramón 182, 20014  
476 Donostia – San Sebastián, Spain. Email: [barroshr@usp.br](mailto:barroshr@usp.br)

477 Fernando López-Gallego - CIC biomaGUNE. Basque Research and Technology Alliance (BRTA),  
478 Paseo de Miramón 182, 20014 Donostia – San Sebastián, Spain; Ikerbasque, Basque Foundation  
479 for Science, 48013 Bilbao, Spain. Email: [flopez@cicbiomagune.es](mailto:flopez@cicbiomagune.es)

480 **Author Contributions**

481 The manuscript was written through contributions of all authors. All authors have given approval  
482 to the final version of the manuscript.

483 **Notes**

484 The authors declare no competing financial interest.

#### 485 ACKNOWLEDGMENT

486 Authors thank Brazilian agencies CNPq and São Paulo Research Foundation FAPESP  
487 (2015/26308-7, 2018/13492-2) for financial support. HRB also thanks FAPESP for the fellowships  
488 granted (2019/09668-0, 2017/20892-4). PHCC thanks FAPESP, the University of Helsinki, and  
489 the Jane and Aatos Erkko Foundation for support. CK thanks funding from the European Union's  
490 Horizon 2020 research and innovation program under the Marie Skłodowska-Curie grant  
491 agreement No. 799393 (NANOBIOME). LML-M and IG acknowledges funding from the Spanish  
492 State Research Agency (Grant MAT2017-86659-R). Funding from IKERBASQUE to LML-M  
493 and FLG is also acknowledged. This work was performed under the Maria de Maeztu Units of  
494 Excellence Program from the Spanish State Research Agency – Grant No. MDM-2017-0720.

#### 495 ABBREVIATIONS

496 Au NPs, gold nanoparticles; AuNSp, gold nanospheres; AuNSt, gold nanostars; CALB, *Candida*  
497 *antarctica* fraction B; CD, circular dichroism; k, rate constant;  $k_{cat}$ , apparent catalytic rate;  $k_{cat}/K_M$ ,  
498 catalytic efficiency; KIE, kinetic isotopic effect;  $K_M$ , Michaelis constant; LSPR, localized surface  
499 plasmon resonance; MRE, mean residue ellipticity; NIR, near-infrared; *p*NP, 4-nitrophenolate;  
500 *p*NPP, 4-nitrophenyl palmitate; TEM, transmission electron microscopy.

501

#### 502 REFERENCES

- 503 1. Mosquera, J.; Zhao, Y.; Jang, H. J.; Xie, N. L.; Xu, C. L.; Kotov, N. A.; Liz-Marzán, L.  
504 M., Plasmonic Nanoparticles with Supramolecular Recognition. *Adv. Funct. Mater.* **2020**, *30*, 1-  
505 17.
- 506 2. Litti, L.; Reguera, J.; de Abajo, F. J. G.; Meneghetti, M.; Liz-Marzán, L. M., Manipulating  
507 Chemistry Through Nanoparticle Morphology. *Nanoscale Horiz.* **2020**, *5*, 102-108.

- 508 3. Bodelón, G.; Costas, C.; Pérez-Juste, J.; Pastoriza-Santos, I.; Liz-Marzán, L. M., Gold  
509 Nanoparticles for Regulation of Cell Function and Behavior. *Nano Today* **2017**, *13*, 40-60.
- 510 4. Liz-Marzán, L. M.; Murphy, C. J.; Wang, J. F., Nanoplasmonics. *Chem. Soc. Rev.* **2014**,  
511 *43*, 3820-3822.
- 512 5. Araujo, T. P.; Quiroz, J.; Barbosa, E. C. M.; Camargo, P. H. C., Understanding Plasmonic  
513 Catalysis with Controlled Nanomaterials Based on Catalytic and Plasmonic Metals *Curr. Opin.*  
514 *Colloid Interface Sci.* **2019**, *39*, 110-122.
- 515 6. Linic, S.; Aslam, U.; Boerigter, C.; Morabito, M., Photochemical Transformations on  
516 Plasmonic Metal Nanoparticles. *Nat. Mat.* **2015**, *14*, 567-576.
- 517 7. Wang, H.; Liu, T.; Huang, Y. Z.; Fang, Y. R.; Liu, R. C.; Wang, S. X.; Wen, W. J.;  
518 Sun, M. T., Plasmon-Driven Surface Catalysis in Hybridized Plasmonic Gap Modes. *Sci. Rep.*  
519 **2014**, *4*.
- 520 8. Baffou, G.; Quidant, R., Thermo-Plasmonics: Using Metallic Nanostructures as Nano-  
521 Sources of Heat. *Laser & Photonics Rev.* **2013**, *7*, 171-187.
- 522 9. Baffou, G.; Quidant, R., Nanoplasmonics for Chemistry. *Chem. Soc. Rev.* **2014**, *43*, 3898-  
523 3907.
- 524 10. Guo, S. J.; Li, H.; Liu, J.; Yang, Y. M.; Kong, W. Q.; Qiao, S.; Huang, H.; Liu, Y.;  
525 Kang, Z. H., Visible-Light-Induced Effects of Au Nanoparticle on Laccase Catalytic Activity. *ACS*  
526 *Appl. Mater. Interfaces* **2015**, *7*, 20937-20944.
- 527 11. Bretschneider, J. C.; Reismann, M.; von Plessen, G.; Simon, U., Photothermal Control of  
528 the Activity of HRP-Functionalized Gold Nanoparticles. *Small* **2009**, *5*, 2549-2553.
- 529 12. Blankschien, M. D.; Pretzer, L. A.; Huschka, R.; Halas, N. J.; González, R.; Wong, M.  
530 S., Light-Triggered Biocatalysis Using Thermophilic Enzyme-Gold Nanoparticle Complexes.  
531 *ACS Nano* **2013**, *7*, 654-663.
- 532 13. Li, W.; Liu, D. N.; Geng, X.; Li, Z. Q.; Gao, R. J., Real-Time Regulation of Catalysis by  
533 Remote-Controlled Enzyme-Conjugated Gold Nanorod Composites for Aldol Reaction-Based  
534 Applications. *Catal. Sci. Technol.* **2019**, *9*, 2221-2230.
- 535 14. Tadepalli, S.; Yim, J.; Madireddi, K.; Luang, J. Y.; Naik, R. R.; Singamaneni, S., Gold  
536 Nanorod-Mediated Photothermal Enhancement of the Biocatalytic Activity of a Polymer-  
537 Encapsulated Enzyme. *Chem. Mater.* **2017**, *29*, 6308-6314.
- 538 15. Tadepalli, S.; Yim, J.; Cao, S. S.; Wang, Z. Y.; Naik, R. R.; Singamaneni, S., Metal-  
539 Organic Framework Encapsulation for the Preservation and Photothermal Enhancement of  
540 Enzyme Activity. *Small* **2018**, *14*.
- 541 16. Yang, S. Y.; Yao, D. F.; Wang, Y. S.; Yang, W. T.; Zhang, B. B.; Wang, D. B., Enzyme-  
542 Triggered Self-Assembly of Gold Nanoparticles for Enhanced Retention Effects and Photothermal  
543 Therapy of Prostate Cancer. *Chem. Commun.* **2018**, *54*, 9841-9844.
- 544 17. Khiavi, M. A.; Safary, A.; Aghanejad, A.; Barar, J.; Rasta, S. H.; Golchin, A.; Omid,  
545 Y.; Somi, M. H., Enzyme-Conjugated Gold Nanoparticles for Combined Enzyme and  
546 Photothermal Therapy of Colon Cancer Cells. *Colloids Surf. A* **2019**, *572*, 333-344.
- 547 18. Yang, K. K.; Liu, Y. J.; Wang, Y.; Ren, Q. L.; Guo, H. Y.; Matson, J. B.; Chen, X. Y.;  
548 Nie, Z. H., Enzyme-Induced in Vivo Assembly of Gold Nanoparticles for Imaging-Guided  
549 Synergistic Chemo-Photothermal Therapy of Tumor. *Biomaterials* **2019**, *223*.
- 550 19. Barros, H. R.; López-Gallego, F.; Liz-Marzán, L. M., Light-Driven Catalytic Regulation  
551 of Enzymes at the Interface with Plasmonic Nanomaterials. *Biochemistry* **2020**, Article ASAP.

- 552 20. Nel, A. E.; Madler, L.; Velegol, D.; Xia, T.; Hoek, E. M. V.; Somasundaran, P.;  
553 Klaessig, F.; Castranova, V.; Thompson, M., Understanding Biophysicochemical Interactions at  
554 the Nano-Bio Interface. *Nat. Mater.* **2009**, *8*, 543-557.
- 555 21. Ansari, S. A.; Husain, Q., Potential Applications of Enzymes Immobilized on/in Nano  
556 Materials: A Review. *Biotechnol. Adv.* **2012**, *30*, 512-523.
- 557 22. Breger, J. C.; Ancona, M. G.; Walper, S. A.; Oh, E.; Susumu, K.; Stewart, M. H.;  
558 Deschamps, J. R.; Medintz, I. L., Understanding How Nanoparticle Attachment Enhances  
559 Phosphotriesterase Kinetic Efficiency. *ACS Nano* **2015**, *9*, 8491-8503.
- 560 23. Breger, J. C.; Oh, E.; Susumu, K.; Klein, W. P.; Walper, S. A.; Ancona, M. G.; Medintz,  
561 I. L., Nanoparticle Size Influences Localized Enzymatic Enhancement-A Case Study with  
562 Phosphotriesterase. *Bioconjugate Chem.* **2019**, *30*, 2060-2074.
- 563 24. de Barros, H. R.; Santos, M. C.; Barbosa, L. R. S.; Piovan, L.; Riegel-Vidotti, I. C.,  
564 Physicochemical Study of the Interaction between Gold Nanoparticles and Lipase from *Candida*  
565 sp. (CALB): Insights into the Nano-Bio Interface. *J. Braz. Chem. Soc.* **2019**, *30*, 2231-2242.
- 566 25. Kisukuri, C. M.; Palmeira, D. J.; Rodrigues, T. S.; Camargo, P. H. C.; Andrade, L. H.,  
567 Bimetallic Nanoshells as Platforms for Metallo- and Biometallo-Catalytic Applications.  
568 *Chemcatchem* **2016**, *8*, 171-179.
- 569 26. Wu, C. S.; Wu, C. T.; Yang, Y. S.; Ko, F. H., An Enzymatic Kinetics Investigation into  
570 the Significantly Enhanced Activity of Functionalized Gold Nanoparticles. *Chem. Commun.* **2008**,  
571 5327-5329.
- 572 27. Baumann, V.; Muhammed, M. A. H.; Blanch, A. J.; Dey, P.; Rodriguez-Fernandez, J.,  
573 Biomolecules in Metal and Semiconductor Nanoparticle Growth. *Isr. J. Chem.* **2016**, *56*, 195-213.
- 574 28. Johnson, B. J.; Algar, W. R.; Malanoski, A. P.; Ancona, M. G.; Medintz, I. L.,  
575 Understanding Enzymatic Acceleration at Nanoparticle Interfaces: Approaches and Challenges.  
576 *Nano Today* **2014**, *9*, 102-131.
- 577 29. Song, Y. H.; Chen, J. Y.; Liu, H. Y.; Song, Y. G.; Xu, F. G.; Tan, H. L.; Wang, L.,  
578 Conformation, Bioactivity and Electrochemical Performance of Glucose Oxidase Immobilized on  
579 Surface of Gold Nanoparticles. *Electrochim. Acta* **2015**, *158*, 56-63.
- 580 30. Lopez-Tobar, E.; Hernandez, B.; Ghomi, M.; Sanchez-Cortes, S., Stability of the  
581 Disulfide Bond in Cystine Adsorbed on Silver and Gold Nanoparticles As Evidenced by SERS  
582 Data. *Journal of Physical Chemistry C* **2013**, *117* (3), 1531-1537.
- 583 31. Hakkinen, H., The Gold-Sulfur Interface at the Nanoscale. *Nat. Chem.* **2012**, *4*, 443-455.
- 584 32. Irani, M.; Tornvall, U.; Genheden, S.; Larsen, M. W.; Hatti-Kaul, R.; Ryde, U., Amino  
585 Acid Oxidation of *Candida antarctica* Lipase B Studied by Molecular Dynamics Simulations and  
586 Site-Directed Mutagenesis. *Biochemistry* **2013**, *52*, 1280-1289.
- 587 33. de Aberasturi, D. J.; Serrano-Montes, A. B.; Langer, J.; Henriksen-Lacey, M.; Parak, W.  
588 J.; Liz-Marzán, L. M., Surface Enhanced Raman Scattering Encoded Gold Nanostars for  
589 Multiplexed Cell Discrimination. *Chem. Mater.* **2016**, *28*, 6779-6790.
- 590 34. Yuan, H. K.; Khoury, C. G.; Hwang, H.; Wilson, C. M.; Grant, G. A.; Vo-Dinh, T., Gold  
591 Nanostars: Surfactant-Free Synthesis, 3D Modelling, and Two-Photon Photoluminescence  
592 Imaging. *Nanotechnology* **2012**, *23*.
- 593 35. Turkevich, J.; Stevenson, P. C.; Hillier, J., A Study of the Nucleation and Growth  
594 Processes in the Synthesis of Colloidal Gold. *Discuss. Faraday Soc.* **1951**, 55-75.
- 595 36. Kheiriloomoo, A.; Khorasheh, F.; Fazelinia, H., Influence of External Mass Transfer  
596 Limitation on Apparent Kinetic Parameters of Penicillin G Acylase Immobilized on Nonporous  
597 Ultrafine Silica Particles. *J. Biosci. Bioeng.* **2002**, *93*, 125-129.

598 37. Kuttner, C.; Holler, R. P. M.; Quintanilla, M.; Schnepf, M. J.; Dulle, M.; Fery, A.; Liz-  
599 Marzan, L. M., SERS and Plasmonic Heating Efficiency from Anisotropic Core/Satellite  
600 Superstructures. *Nanoscale* **2019**, *11*, 17655-17663.

601 38. Hendel, T.; Wuithschick, M.; Kettemann, F.; Birnbaum, A.; Rademann, K.; Polte, J., In  
602 Situ Determination of Colloidal Gold Concentrations with UV-Vis Spectroscopy: Limitations and  
603 Perspectives. *Anal. Chem.* **2014**, *86*, 11115-11124.

604 39. Daniel, R. M.; Danson, M. J., Temperature and the Catalytic Activity of Enzymes: A Fresh  
605 Understanding. *FEBS Letters* **2013**, *587*, 2738-2743.

606 40. Rabbani, G.; Ahmad, E.; Khan, M. V.; Ashraf, M. T.; Bhat, R.; Khan, R. H., Impact of  
607 Structural Stability of Cold Adapted *Candida antarctica* Lipase B (CALB): In Relation to pH,  
608 Chemical and Thermal Denaturation. *RSC Adv.* **2015**, *5*, 20115-20131.

609 41. Armenia, I.; Bonavia, M. V. G.; De Matteis, L.; Ivanchenko, P.; Martra, G.; Gornati,  
610 R.; de la Fuente, J. M.; Bernardini, G., Enzyme Activation by Alternating Magnetic Field:  
611 Importance of the Bioconjugation Methodology. *J. Colloid Interface Sci.* **2019**, *537*, 615-628.

612 42. Jain, P. K., Taking the Heat Off of Plasmonic Chemistry. *J. Phys. Chem. C* **2019**, *123*,  
613 24347-24351.

614 43. Chatterjee, H.; Rahman, D. S.; Sengupta, M.; Ghosh, S. K., Gold Nanostars in Plasmonic  
615 Photothermal Therapy: The Role of Tip Heads in the Thermoplasmonic Landscape. *J. Phys. Chem.*  
616 *C* **2018**, *122*, 13082-13094.

617 44. Leitner, D. M.; Pandey, H. D.; Reid, K. M., Energy Transport across Interfaces in  
618 Biomolecular Systems. *J. Phys. Chem. B* **2019**, *123*, 9507-9524.

619 45. Johnson, K. A., A Century of Enzyme Kinetic Analysis, 1913 to 2013. *FEBS Letters* **2013**,  
620 *587*, 2753-2766.

621 46. Powers, K. T.; Washington, M. T., *Analyzing the Catalytic Activities and Interactions of*  
622 *Eukaryotic Translesion Synthesis Polymerases*. 1<sup>st</sup> edition; Academic Press 2017, Vol. 592.

623 47. Hammes, G.; Hammes-Schiffer, S., *Physical Chemistry for the Biological Sciences*. 2nd  
624 edition ed.; John Wiley & Sons; New Jersey, 2015; Vol. 55.

625 48. Gadda, G.; Fitzpatrick, P. F., Solvent Isotope and Viscosity Effects on the Steady-State  
626 Kinetics of the Flavoprotein Nitroalkane Oxidase. *FEBS Letters* **2013**, *587*, 2785-2789.

627 49. Jaeger, K. E.; Dijkstra, B. W.; Reetz, M. T., Bacterial Biocatalysts: Molecular Biology,  
628 Three-Dimensional Structures, and Biotechnological Applications of Lipases. *Annu. Rev.*  
629 *Microbiol.* **1999**, *53*, 315-351.

630 50. Telis, V. R. N.; Telis-Romero, J.; Mazzotti, H. B.; Gabas, A. L., Viscosity of Aqueous  
631 Carbohydrate Solutions at Different Temperatures and Concentrations. *Int. J. Food Prop.* **2007**,  
632 *10*, 185-195.

633 51. Galmes, M. A.; Garcia-Junceda, E.; Swiderek, K.; Moliner, V., Exploring the Origin of  
634 Amidase Substrate Promiscuity in CALB by a Computational Approach. *ACS Catal.* **2020**, *10*,  
635 1938-1946.

636 52. Hoops, S.; Sahle, S.; Gauges, R.; Lee, C.; Pahle, J.; Simus, N.; Singhal, M.; Xu, L.;  
637 Mendes, P.; Kummer, U., COPASI- A COMplex PATHway SIMulator. *Bioinformatics* **2006**, *22*,  
638 3067-3074.

639 53. Quinn, D. M., Solvent Isotope Effects for Lipoprotein-Lipase Catalyzed-Hydrolysis of  
640 Water-Soluble para-Nitrophenyl Esters. *Biochemistry* **1985**, *24*, 3144-3149.

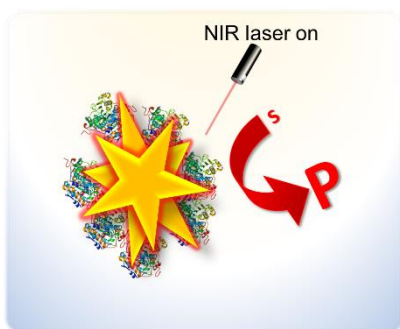
641 54. Bradford, M. M., Rapid and Sensitive Method for Quantitation of Microgram Quantities  
642 of Protein Utilizing Principle of Protein-Dye Binding. *Anal. Biochem.* **1976**, *72*, 248-254.

643 55. Bastus, N. G.; Comenge, J.; Puentes, V., Kinetically Controlled Seeded Growth Synthesis  
644 of Citrate-Stabilized Gold Nanoparticles of up to 200 nm: Size Focusing versus Ostwald Ripening.  
645 *Langmuir* **2011**, *27*, 11098-11105.

646 56. Johnson, K. A.; Goody, R. S., The Original Michaelis Constant: Translation of the 1913  
647 Michaelis-Menten Paper. *Biochemistry* **2011**, *50*, 8264-8269.

648

649 FOR TABLE OF CONTENTS ONLY



650

651 **Plasmonic biocatalysis:** control of enzyme activity by LSPR excitation of plasmonic  
652 nanoparticles using external light irradiation.